2024 6th International Conference on Reconfigurable
Mechanisms and Robots (ReMAR)
June 24-27, 2024. Chicago, IL, USA

Active Surface with Passive Omni-Directional Adaptation for In-Hand Manipulation

Sen Li[1], Fang Wan[2,*], and Chaoyang Song[3,*]

2024 6th International Conference on Reconfigurable Mechanisms and Robots (ReMAR) | 979-8-3503-9596-9/24/$31.00 ©2024 IEEE | DOI: 10.1109/REMAR61031.2024.10619925

***Abstract*— Soft fingers with omni-directional adaptability excel in 3D twisting, outperforming two-dimensional self-adaptive hands using a finger rotation mechanism to achieve similar adaptability. In this study, we present the design of a soft robotic finger with an active surface on an omni-adaptive structure, which can be easily installed on existing grippers and achieve stability and dexterity for in-hand manipulation. The system's active surfaces initially transfer the object from the fingertip segment with less compliance to the middle segment of the finger with superior adaptability. Despite the omni-directional deformation of the finger, in-hand manipulation can still be executed with controlled active surfaces. We characterized the soft finger's stiffness distribution and simplified models to assess the feasibility of lifting and reorienting a grasped object in a 3D twisting state. A set of experiments on in-hand manipulation was performed with the proposed fingers, demonstrating the dexterity and robustness of the strategy.**

I. Introduction

Manipulation and locomotion share morphological intelligence fostered by the evolutional adaptation to the complex environment, which can also be achieved in robotic systems through evolutionary reinforcement learning [1], [2]. Land-based robotic locomotion takes the form of wheeled, legged, or tracked mobility [3]. Tracks are designed to distribute loads and enhance traction and maneuverability on loose surfaces, thanks to the larger contact areas, compared to wheeled and legged locomotions. Likewise, robotic in-hand manipulation tasks can also be categorized by how the fingers contact and drive the object to the target pose.

Legged locomotion and precision grasp (with fixed contact at fingertip) for in-hand manipulation share the advantage of transversality and dexterity, respectively, and smaller footprint or contact area. Robotic grippers adopting such a strategy take the form of a multi-finger humanoid hand [4], [5], [6], [7], [8], [9] and require more dedicated perception and planning algorithms to achieve stability. A popular approach is to attach tactile sensors [10], [11] to fingertips, further increasing the complexity and cost of the robotic hand. Like wheeled locomotion, a precision grasp with rolling contact aims to increase stability while maintaining dexterity through gripper design [12], [13], [14].

The counterpart to tracked mobility in manipulation uses active surfaces [15]. Grippers with active surfaces can drive the grasped object while maintaining continuous contact, providing higher stability and lower dexterity than the former two categories. Like the tracked mobility counterpart, most active surfaces encompass rigid or fully actuated fingers [16], [17], [18]. Contrary to locomotion tasks where terrain usually varies at a larger spatial scale than the tracks, in-hand manipulation deals with objects smaller than or comparable to the finger size. The active surface over a rigid finger is inefficiently utilized, especially when the shape of an object is curved, and only a tiny portion of the surface is in contact with the object.

Soft robotic hands [19] made from compliant materials [20] or structures [21] can adapt to the grasped objects in irregular shapes or delicate textures and achieve robustness at low cost. Recent work proposed an omni-adaptive soft network structure [22], [23], which differs from fin-ray finger [24], [25] by providing a distinct twisting along the central axis. Their multi-finger grippers demonstrated robust power grasps. However, soft hands are usually challenging to control due to their infinite degrees of freedom, leading to a lack of dexterity. Recent works use compliant fingers with active surfaces [26], [27] to increase dexterity in soft hands, which shows the potential to achieve simultaneous benefits of adaptability, stability, and dexterity.

This paper proposes a novel soft finger with both passive omni adaptation and active surface to achieve robustness and dexterity for in-hand manipulation. The modularized soft fingers can be easily mounted on a commercial rigid gripper, enabling it for compliant grasping and in-hand manipulation, as shown in Fig.1. Details of the design and experimental platform are described in Section-II. The analysis of the grasping strategy is discussed in Section-III. Section-IV demonstrates and evaluates the grasping and in-hand manipulation tasks on four types of objects. Finally, concluding remarks are included in Section-V.

II. Gripper Design

A. Passive Soft Polyhedral Finger Design

Inspired by the polyhedron [28], [29] and the two-dimensional (2D) self-adaptive finger (such as the Festo MultiChoiceGripper) [30], our design, shown in Fig. 1(a), incorporates a hollow structure to accommodate internal

This work was partly supported by the Ministry of Science and Technology of China [2022YFB4701200], the National Natural Science Foundation of China [62206119], the Science, Technology, and Innovation Commission of Shenzhen Municipality [JCYJ20220818100417038], Shenzhen Long-Term Support for Higher Education at SUSTech [20231115141649002], SUSTech Virtual Teaching Lab for Machine Intelligence Design and Learning [Y01331838]. Corresponding Emails: wanf@sustech.edu.cn (F.W.), songcy@ieee.org (C.S.).

[1]Sen Li is with the School of Design, Southern University of Science and Technology, Shenzhen 518055, China

[2]Fang Wan is with Shenzhen Key Laboratory of Intelligent Robotics and Flexible Manufacturing, Southern University of Science and Technology, Shenzhen, Guangdong 518055, China.

[3]Chaoyang Song is with the Department of Mechanical and Energy Engineering, Southern University of Science and Technology, Shenzhen 518055, China.

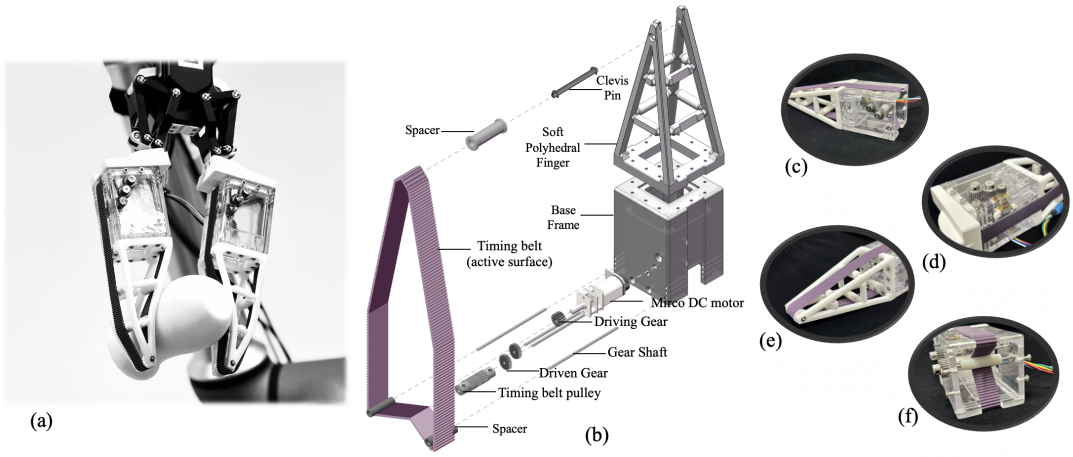

Fig. 1. **Design overview of the proposed soft finger with an active surface.** (a) The soft robotic finger with an active surface on an omni-adaptive structure can be easily installed on existing grippers, achieving stable and dexterous in-hand manipulation. (b) Assembly of mechanical components of the design. (c) Whole soft finger system, with active surface and passive omni-directional adaptation; (d) Physical power systems, encompassing motors and gearing mechanisms; (e) The active finger surface and the soft polyhedral finger; and (f) Active gear transmission mechanism in robotic systems.

vision systems, eliminating the need for external vision enhancements. We've achieved a design combining compliance and strength by transforming the polyhedron's edges into a beam framework to craft a contoured skeleton and integrating cross beams internally. The selection of two-layer beams in our final model offers an optimal compromise, ensuring both flexibility and durability essential for the intended three-dimensional (3D) self-adaptive finger application. The beams at the top were replaced with clevis pins, through which passive rolling guidance was provided. Fig. 1 illustrated the primary design features. Main interaction surfaces intended for typical grasping and secondary interaction surfaces designed for spatial adaptability, such as 3D twisting, are characterized in this design.

We employed a polyurethane elastomer (Hei-cast 8400 from H&K) with a three-component mix ratio of 1:1:0 to attain consistent and stable performance. The entire lattice was fabricated through vacuum molding, achieving a hardness of 90A. The soft polyhedral finger in Fig. 1(e) was chosen as the experimental platform because it has excellent 3D adaptations and fulfills the passive omnidirectional adaptation requirements. The soft polyhedral finger weighs 42 g, stands at a height of 125 mm, and has a base width of 54 mm. We mounted the finger on the base frame, which was 3D-printed from photosensitive resin and weighed 85 g. It also provides installation spaces for components such as the timing belt and the motor drive system.

B. Active Surface Design

An active surface mechanism is incorporated in each soft polyhedral finger. Each active surface mechanism consists of four parts: a timing belt part, a timing belt pulley, a driving gear part, and a driven part.

The timing belt, as depicted in Fig. 1(e), functions analogously to a tank's track, influencing the motion of the grasped object. Each timing belt is constructed using polyurethane elastomers (TPU) with a hardness of 90A. With a modest weight of 10.33 g, its optimal stiffness and damping characteristics allow it effectively to exert a high contact force on objects. The timing belt pulley is manufactured through 3D printing from a high-toughness resin and weighs 2.08 g. The timing belt has a width of 16.5 mm and a thickness ranging from 1 mm to a maximum of 2 mm.

Comprising mainly a Mirco DC motor and the timing belt pulley, the driving part plays a pivotal role in the system. Each driving gear weighs 6.24 g. The driven part enhances system functionality to facilitate the smooth roll motion of the timing belt. Each driving gear has a mass of 1.66 g.

III. Analysis

This section presents details of the interaction between the finger and active surface, stiffness distribution, and system dynamics model. The related parameters of the whole soft finger system are listed in Table I.

TABLE I
Specification of Model for Anyalysis

Character	Definition
m_c	Grasped object mass (kg)
I	Grasped object mass moment of inertia
v_R	Velocity of the right timing belt (m/s)
v_L	Velocity of the left timing belt (m/s)
R	Radius of the grasped object (m)
K_n	P parameter of normal force (N/m)
D_n	D parameter of normal force (N.s/m)
h_f	Displacement of contact point
D_s	P parameter of shear force (N.s/m)

A. Finger-Active Surface Interaction

We investigated how the active surface's movement would affect the finger's compliance. Since the active surface comes into direct contact with the finger's backbone, friction inevitably occurs when it moves relative to the surface of the mechanical finger's backbone. As shown in Fig. 2(b)-(e),

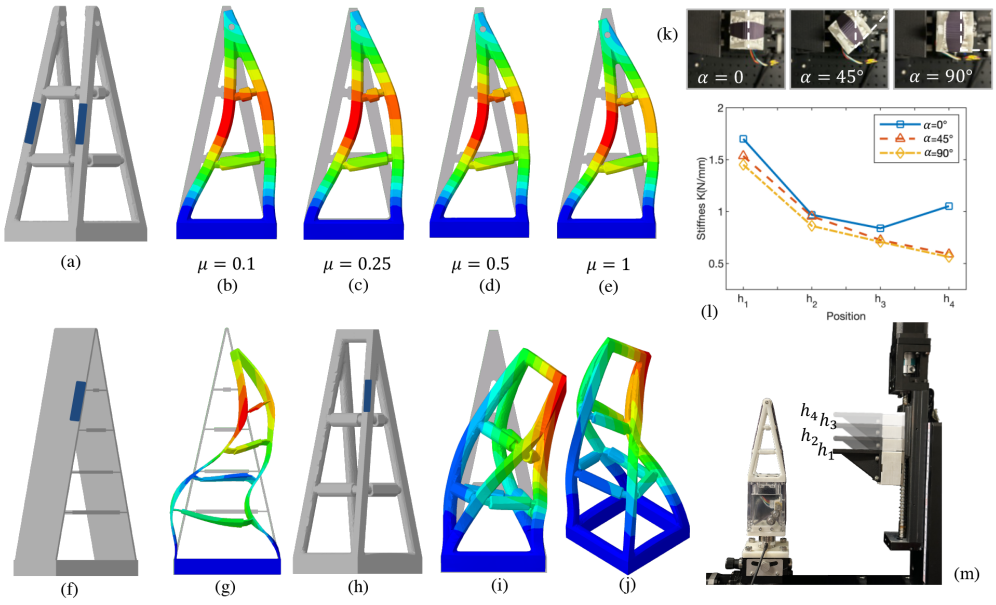

Fig. 2. **The Finite Element Method (FEM) simulation and stiffness distribution of the soft finger.** (a) Simulation setup where contact force is applied to the finger surface. (b)-(e) Comparison of finger deformations with different friction. (f)&(h) Simulation setup where contact force is applied to the 2D Fin Ray finger & 3D self-adaptive finger surface. (g) Deformation result of 2D Fin Ray finger. (i)-(j) Different perspectives of deformation result of 3D self-adaptive finger. The stiffness distribution of the soft polyhedral finger was measured using the test rig. (k) Three distinct propulsion angles, (l) stiffness distribution of soft polyhedral finger with an active surface, and (m) experiment setup for measuring stiffness.

the friction from the active surface has a minimal impact on the finger's compliance unless the coefficient of friction is exceptionally high. Given that the inner surface of the conveyor belt is sufficiently smooth, our analysis leads us to expect that the deviation caused by friction will be minor. Therefore, we can disregard the impact of the active surface and base our subsequent discussions on the structure of the soft polyhedral finger.

B. Passive Finger Compliance: Stiffness Distribution

We conducted a series of unidirectional compression tests to estimate the stiffness distribution of soft polyhedral fingers characterized by the relationship between force and displacement. As illustrated in Fig. 2(m), the soft finger is mounted atop a custom test rig equipped with a high-performance force sensor (ATI Nano25) featuring two motorized linear motions and two manual rotary motions. The probe compressed the soft polyhedral finger horizontally at a rate of 5 mm/s with a predefined depth of 15 mm. Tests were conducted at three distinct propulsion angles.

Experiments were carried out at three distinct propulsion angles: $\theta = 0°$, $\theta = 45°$, and $\theta = 90°$, shown as Fig. 2(k). The measurement results exhibited consistent trends where a decrease in stiffness distribution suggested that the edges of the soft finger possess moderate adaptability, showcasing adaptiveness in three-dimensional space. For all experiments, Fig. 2(l) depicts the decline of stiffness distribution along the z-axis from h_1 to h_4 for angles $\theta = 45°$, and $\theta = 90°$. However, at an angle $\theta = 0°$, the stiffness decreases from 1.699 N/mm at h_1 to 0.838 N/mm at h_3, with a slight increase to 1.051 N/mm at h_4. This distinct stiffness distribution contrasts with the 2D fin ray effect finger, where fingertip stiffness falls to roughly 25% of the base's stiffness [31].

To verify the in-hand manipulation capabilities with the newly introduced omnidirectional adaptive fingers, an active surface design with passive omnidirectional adaptation was demonstrated by building the experimental platform described in this section. The proposed in-hand manipulation technique prototype, shown in Fig. 1(a), has mainly three parts: a DH-AG95 gripper, two passive soft polyhedral fingers, and two active surfaces.

C. Comparison with 2D FinRay Finger

We also compared the deformation during twisting between the proposed 3D self-adaptive finger and the 2D FinRay finger in the FEM simulation. This comparison was chosen because twisting represents a significant vulnerability of the 2D FinRay finger. At the same time, certain commercial robotic hands (such as the Festo MultiChoiceGripper) address this weakness by rotating the fingers [27], thereby switching the radial hand to a three-finger parallel configuration and then switching back when necessary using a separate mechanism. To test the performance comparison between the 2D FinRay finger and the 3D self-adaptive finger, we applied contact forces at the same contact positions, as shown in Fig. 2(g),(i)-(j). Compared to the 2D FinRay finger, the 3D self-adaptive finger demonstrated significantly better 3D twisting capabilities.

D. Pinch & Lift Phase in Simplified Model

As illustrated in Fig. 3(b), the pinch phase begins with the robotic fingers approaching the object to be grasped.

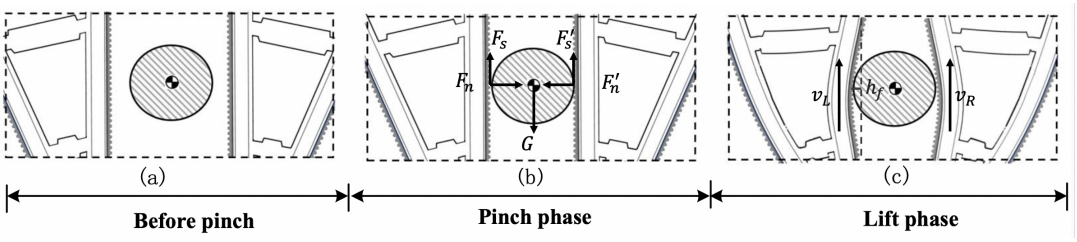

Fig. 3. **Contact model between the grasped object and the belt.** (a) the initial state of the system, (b) pinching one object without breaking and dropping, (c) lifting an object by actuating the belts.

Then, during the lift phase, shown in Fig. 3(c), the gripper slowly closes to allow the belt's surface to contact the object. The belt is then driven at a constant speed to roll up. Upon contact, the object is moved upwards by the moving belt. Slippage is the displacement difference between the object and the belt. Slippage, denoted as δ_{slip}, is calculated as the displacement discrepancy between the object and the belts. The object's displacement should match the belt's displacement to prevent slippage.

The slippage over which the object rolls is determined as follows:

$$\delta_{slip} = \int_{t_1}^{t_2} v_L(t)dt - \int_{t_1}^{t_2} v_R(t)dt \tag{1}$$

The rotational variation, $\delta_{rot} = \frac{\delta_{slip}}{R}$, is represented by the cumulative changes in orientation from the onset of the pinch phase.

The contact between the grasped object and the finger surface is modeled using a spring damper at each contact point. The contact model is described below. In the normal direction of the finger surface, the normal force F_n in the direction $\hat{x}_n$ is modeled by the following equation [32]:

$$F_n = \begin{cases} -(K_n h_f + D_n \dot{h_f}) \cdot \hat{x}_n & h_f \leq 0 \\ 0 & else \end{cases} \tag{2}$$

In the shear direction of the finger surface, friction F_s in the direction $\hat{z}_n$ is modeled using a damper, and it can be expressed as:

$$F_s = \begin{cases} -D_s \dot{h_f} \cdot \hat{z}_n & h_f \leq 0 \\ 0 & else \end{cases} \tag{3}$$

Fig. 3(c) shows the object held by two fingers after the pinch phase. b denotes the body frame of the grasped object. The hypotheses for this simplified model are as follows: a) friction is present between the object and the dual belts, b) air resistance is disregarded in this model, and c) the upward motion of the belt is conventionally defined as the positive direction. The dynamics of this system are:

$$m_c {}^b\ddot{x} = F_s + F_{s'} - m_c g \tag{4}$$

Owing to the differential velocities of the two belts, the frictional forces they exert induce a rotation about the object's axis. Treating the object as a rigid body undergoing rotation about a fixed axis, its moment of inertia, I, can be taken as a known value. The object's angular acceleration, $\ddot{\theta}$, can be determined by the torque, τ, and its moment of inertia. The torque arising from frictional forces can be characterized using the frictional force and the object's radius, R. Given the friction exerted by the belts on the object, the resulting torque can be expressed:

$$I\ddot{\theta} = R \times (F_s - F_{s'}) \tag{5}$$

Thus, the relative velocities of the conveyor belts and their friction coefficients dictate the grasped object's rotational velocity and direction. Meanwhile, the grasped object's vertical motion is governed by the balance between its gravitational force and the combined frictional forces from both belts.

The equilibrium between the dual frictional forces and gravitational force primarily determines the vertical motion of the object. When the belts accelerate upwards, and if the resulting frictional force surpasses the gravitational pull on the object, the object will accelerate upwards in unison with the belts. Conversely, if the belts accelerate downward and the frictional force is insufficient to counteract the object's weight, the object will descend with the belts. In scenarios where the belts decelerate or come to a halt, the diminished frictional force might not be adequate to sustain the object's weight, leading it to slide downward unless otherwise counteracted.

Assuming an object is grasped at the midpoint between the two fingers, $G_{max} = \frac{2\mu_{bo}\tau_m}{L_c}$ is estimated to be the maximum weight of the grasped object. Here, μ_{bo} represents the friction coefficient between the timing belt and the object, $\tau_m = 3.4$ kg$\cdot$ cm is the maximum torque output of the motor, and L_c is the distance between the motor's output shaft and the point of contact on the finger. Taking $\mu_{bo} = 0.5$, the maximum weight of the object that can be grasped is determined to be approximately 0.57 kg.

IV. Results and Discussions

Experiments confirming the effectiveness of the proposed strategy for in-hand manipulation were conducted using four distinct objects: a cube, an irregular 3D-printed vase, a cylinder, and a sphere. These objects varied in shape and size, with the cube weighing 8.66 g and measuring 25.00 mm in length, the irregular object (vase) weighing 132.04 g and 120.00 mm long, the cylinder at 31.74 g and 112.70 mm in length, and the sphere weighing 42.15 g with a diameter of 55.00 mm.

As shown in Figs. 4(a)&(b), the lift strategy was successfully applied to a cube and an irregular 3D-printed vase,

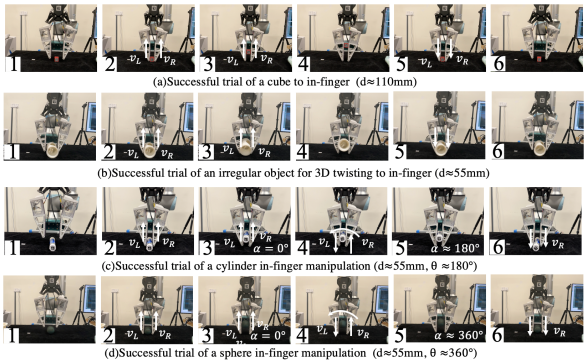

Fig. 4. **Back-to-back experiment (left to right, top to bottom).** (a) and (b) experimental initial condition: displacement d was set to 110 mm and 55 mm, respectively. (c) and (d) experimental initial condition: displacement was set to 55mm, rotation angle θ was set to 180° and 360°, respectively.

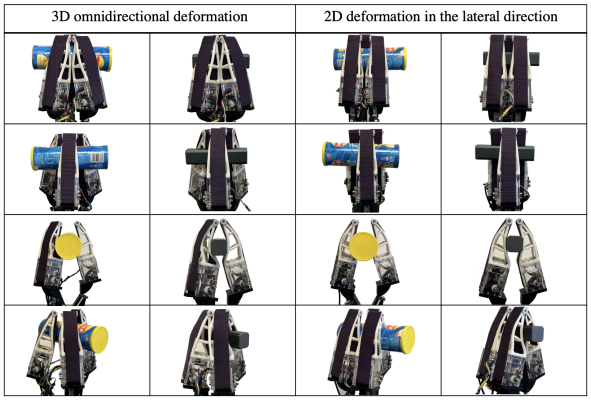

Fig. 5. **Snapshots of 3D omnidirectional deformation grasping using a 3D self-adaptive finger compared with 2D deformation in the lateral direction grasping using the same self-adaptive finger.**

respectively. In the successive snapshots of a successful lifting, the contact occurs, and the object interacts with the belt as it is pressurized. From the second to the fourth snapshot, as the entire object was lifted, the kinetic energy of the belt was converted into the gravitational potential energy of the grasped object. In the fourth panel, the pull-in phase terminates, and the push-out phase begins. The object falls under the controlled belt in the fifth and sixth panels. We further tested the robustness of the lift by conducting each experiment 20 times. The cube was successfully repositioned to the middle segment in 20/20 trials.. The irregular vase was successfully grasped and repositioned in 14/20 trials.

Lifting and reorientation were tested on a cylinder and a sphere. Figs. 4(c)&(d) show successive snapshots of successful in-hand manipulations of a cylinder and sphere, respectively, in the second snapshot of Figs. 4(c)&(d), the contact begins, and the object interacts with the belt as it is pressurized. From the second to the third snapshot, as the entire object was lifted to the middle of the finger, the kinetic energy of the belt was converted into the gravitational potential energy of the grasped object. In the fourth snapshot, the lift phase terminates, and the reorientation phase begins. In the fifth snapshot, the orientation phase terminates, and the push-out phase of orientation begins. The object falls under the controlled belt in the fifth and sixth snapshots, while the gravitational potential energy is converted to kinetic energy.

As shown in Fig. 4(c), the cylinder was successfully reorientated in 16/20 trials. As shown in Fig. 4(d), the sphere was successfully reorientated in 20/20 trials. The experimental results verify that the proposed in-hand manipulation strategy works effectively while maintaining a stable grasp. Fig. 6 indicates that the trend of the displacement at a cylinder and the sphere is consistent. The grasped object rotated after reaching the middle of the soft polyhedral finger and started rotating under gravity and the contact force.

Besides being applied to the planar two-finger configuration of in-hand manipulation, it can also be extended to a three-finger configuration, demonstrating omnidirectional deformation and grasping of objects with irregular shapes. During testing, it was observed that mechanical fingers based on a two-dimensional design struggle to make good contact with objects. In contrast, fingers of a 3D omnidirectional soft finger design can adapt to the shapes of prisms and cylinders in different ways and grasp them firmly. In tests of 3D omnidirectional deformation capabilities, when the fingers contact a rectangular prism and a cylinder simultaneously, they deform in multiple directions, automatically transitioning to a grip configuration similar to parallel gripping while still closely conforming to the object's shape. As shown in Fig. 5, the deformation of the soft fingers of a 3-finger radial gripper when grasping prisms and cylinders is visible.

In contrast, during tests of 2D deformation in the lateral direction, the gripping method of the 2D mechanical hand requires rotating the fingers to switch the gripper from a radial to a three-finger parallel configuration, allowing the finger surfaces to contact the rectangular prisms and cylinders. This process requires an additional mechanism to switch back and forth between configurations.

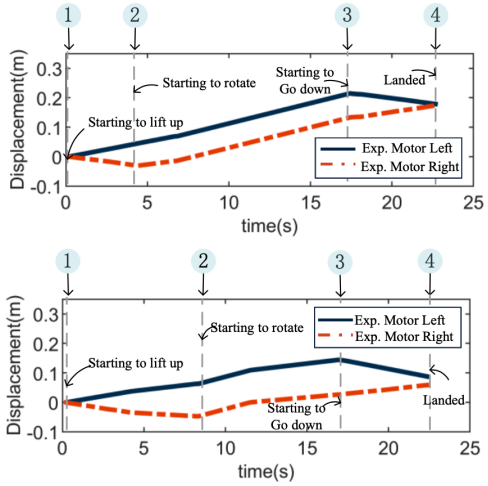

Fig. 6. **Experimental displacement data were obtained from successful trials involving (Top) a cylinder and (Bottom) a sphere.** The key timing is as follows: contact and start to lift at ①, orientation begins at ②, downward movement happens during ③-④, and stable placement at ④.

V. Conclusion

This paper presents a soft finger design for stability and dexterity for in-hand manipulation. Two key design strategies achieve this: the soft polyhedral structure with 3D omni-adaptability and the active surface covering the soft structure, offering extra dexterity. Two proposed fingers were used to augment a commercial rigid gripper and enable it to perform 3D omni-adaptability without a rotation mechanism. To in-hand manipulation, the grasped object can be lifted with active surfaces and reoriented without needing environmental assistance or reliance on push-and-grasp techniques. The omni-adaptability extends previous works on active surfaces by enhancing grasping stability and flexibility. Experiments on the in-hand manipulation tasks show that the finger design works well for objects with irregular items.

There were some trials in which the object failed to be in hand. The main reason may be that the beam of the soft finger was too convex when the contact happened, causing one side of the object to move faster than expected. Some qualitative conclusions are that, as the contact area and force increase, the belt's width and the groove's depth must follow to ensure that. However, such a design may not be realistic for belts to handle large loads because of the excessive motor torque required. Key factors for quantitative analysis are beam count and dimensions. Having an excessive number and scale of beams could compromise the structure's flexibility and lead to visual obstruction. Conversely, a scarcity of beams may fail to offer sufficient support.

References

[1] A. Gupta, S. Savarese, S. Ganguli, and L. Fei-Fei, "Embodied intelligence via learning and evolution," *Nature communications*, vol. 12, no. 1, p. 5721, 2021.

[2] H. Sun, L. Yang, Y. Gu, J. Pan, F. Wan, and C. Song, "Bridging locomotion and manipulation using reconfigurable robotic limbs via reinforcement learning," *Biomimetics*, vol. 8, no. 4, 2023.

[3] F. Rubio, F. Valero, and C. Llopis-Albert, "A review of mobile robots: Concepts, methods, theoretical framework, and applications," *International Journal of Advanced Robotic Systems*, vol. 16, no. 2, p. 1729881419839596, 2019.

[4] S. Abondance, C. B. Teeple, and R. J. Wood, "A dexterous soft robotic hand for delicate in-hand manipulation," *IEEE Robotics and Automation Letters*, vol. 5, no. 4, pp. 5502–5509, 2020.

[5] O. M. Andrychowicz, B. Baker, M. Chociej, R. Józefowicz, B. McGrew, J. Pachocki, A. Petron, M. Plappert, G. Powell, A. Ray, J. Schneider, S. Sidor, J. Tobin, P. Welinder, L. Weng, and W. Zaremba, "Learning dexterous in-hand manipulation," *The International Journal of Robotics Research*, vol. 39, no. 1, pp. 3–20, 2020.

[6] C. M. McCann and A. M. Dollar, "Design of a stewart platform-inspired dexterous hand for 6-dof within-hand manipulation," in *2017 IEEE/RSJ International Conference on Intelligent Robots and Systems (IROS)*, 2017, pp. 1158–1163.

[7] G. Wei, J. S. Dai, S. Wang, and H. Luo, "Kinematic analysis and prototype of a metamorphic anthropomorphic hand with a reconfigurable palm," *International Journal of Humanoid Robotics*, vol. 8, no. 03, pp. 459–479, 2011.

[8] H. Dong, E. Asadi, C. Qiu, J. Dai, and I.-M. Chen, "Geometric design optimization of an under-actuated tendon-driven robotic gripper," *Robotics and Computer-Integrated Manufacturing*, vol. 50, pp. 80–89, 2018.

[9] J. S. Dai, D. Wang, and L. Cui, "Orientation and workspace analysis of the multifingered metamorphic hand—metahand," *IEEE Transactions on Robotics*, vol. 25, no. 4, pp. 942–947, 2009.

[10] W. Yuan, S. Dong, and E. H. Adelson, "Gelsight: High-resolution robot tactile sensors for estimating geometry and force," *Sensors*, vol. 17, no. 12, p. 2762, 2017.

[11] Y. Yan, Z. Hu, Z. Yang, W. Yuan, C. Song, J. Pan, and Y. Shen, "Soft magnetic skin for super-resolution tactile sensing with force self-decoupling," *Science Robotics*, vol. 6, no. 51, p. eabc8801, 2021.

[12] S. Yuan, A. D. Epps, J. B. Nowak, and J. K. Salisbury, "Design of a roller-based dexterous hand for object grasping and within-hand manipulation," in *2020 IEEE International Conference on Robotics and Automation (ICRA)*, 2020, pp. 8870–8876.

[13] S. Yuan, L. Shao, C. L. Yako, A. Gruebele, and J. K. Salisbury, "Design and control of roller grasper v2 for in-hand manipulation," in *2020 IEEE/RSJ International Conference on Intelligent Robots and Systems (IROS)*, 2020, pp. 9151–9158.

[14] J. M. Gómez-de Gabriel and H. A. Wurdemann, "Adaptive underactuated finger with active rolling surface," *IEEE Robotics and Automation Letters*, vol. 6, no. 4, pp. 8253–8260, 2021.

[15] V. Tincani, M. G. Catalano, E. Farnioli, M. Garabini, G. Grioli, G. Fantoni, and A. Bicchi, "Velvet fingers: A dexterous gripper with active surfaces," in *2012 IEEE/RSJ International Conference on Intelligent Robots and Systems*. IEEE, 2012, pp. 1257–1263.

[16] *In-Hand Manipulation Primitives for a Minimal, Underactuated Gripper With Active Surfaces*, ser. International Design Engineering Technical Conferences and Computers and Information in Engineering Conference, vol. Volume 5A: 40th Mechanisms and Robotics Conference, 08 2016.

[17] A. Kakogawa, H. Nishimura, and S. Ma, "Underactuated modular finger with pull-in mechanism for a robotic gripper," in *2016 IEEE International Conference on Robotics and Biomimetics (ROBIO)*, 2016, pp. 556–561.

[18] A. J. Spiers, B. Calli, and A. M. Dollar, "Variable-friction finger surfaces to enable within-hand manipulation via gripping and sliding," *IEEE Robotics and Automation Letters*, vol. 3, no. 4, pp. 4116–4123, 2018.

[19] J. Shintake, V. Cacucciolo, D. Floreano, and H. Shea, "Soft robotic grippers," *Advanced materials*, vol. 30, no. 29, p. 1707035, 2018.

[20] T. G. Thuruthel, B. Shih, C. Laschi, and M. T. Tolley, "Soft robot perception using embedded soft sensors and recurrent neural networks," *Science Robotics*, vol. 4, no. 26, p. eaav1488, 2019.

[21] B. Wang, W. Guo, S. Feng, Y. Hongdong, F. Wan, and C. Song, "Volumetrically enhanced soft actuator with proprioceptive sensing," *IEEE Robotics and Automation Letters*, vol. 6, no. 3, pp. 5284–5291, 2021.

[22] F. Wan, H. Wang, J. Wu, Y. Liu, S. Ge, and C. Song, "A reconfigurable design for omni-adaptive grasp learning," *IEEE Robotics and Automation Letters*, vol. 5, no. 3, pp. 4210–4217, 2020.

[23] L. Yang, F. Wan, H. Wang, X. Liu, Y. Liu, J. Pan, and C. Song, "Rigid-soft interactive learning for robust grasping," *IEEE Robotics and Automation Letters*, vol. 5, no. 2, pp. 1720–1727, 2020.

[24] X. Shan and L. Birglen, "Modeling and analysis of soft robotic fingers using the fin ray effect," *The International Journal of Robotics Research*, vol. 39, no. 14, pp. 1686–1705, 2020.

[25] W. Xu, H. Zhang, H. Yuan, and B. Liang, "A compliant adaptive gripper and its intrinsic force sensing method," *IEEE Transactions on Robotics*, vol. 37, no. 5, pp. 1584–1603, 2021.

[26] N. Govindan and A. Thondiyath, "Design and Analysis of a Multimodal Grasper Having Shape Conformity and Within-Hand Manipulation With Adjustable Contact Forces," *Journal of Mechanisms and Robotics*, vol. 11, no. 5, p. 051012, 07 2019.

[27] Y. Cai and S. Yuan, "In-hand manipulation in power grasp: Design of an adaptive robot hand with active surfaces," in *2023 IEEE International Conference on Robotics and Automation (ICRA)*, 2023, pp. 10 296–10 302.

[28] E. D. Demaine and J. O'Rourke, *Geometric folding algorithms: linkages, origami, polyhedra*. Cambridge university press, 2007.

[29] G. Wei and J. S. Dai, "A spatial eight-bar linkage and its association with the deployable platonic mechanisms," *Journal of Mechanisms and Robotics*, vol. 6, no. 2, p. 021010, 2014.

[30] Festo Corporate, "MultiChoiceGripper," https://www.festo.com, 2013, [Online; accessed 19-Feb-2024].

[31] X. Shan and L. Birglen, "Modeling and analysis of soft robotic fingers using the fin ray effect," *The International journal of robotics research*, vol. 39, no. 14, pp. 1686–1705, 2020.

[32] A. Ghafoor, J. S. Dai, and J. Duffy, "Stiffness modeling of the soft-finger contact in robotic grasping," *J. Mech. Des.*, vol. 126, no. 4, pp. 646–656, 2004.